AFRL-VA-WP-TP-2007-303

FAULT TOLERANT OPTIMAL TRAJECTORY GENERATION FOR REUSABLE LAUNCH VEHICLES (PREPRINT)

Patrick J. Shaffer, I. Michael Ross, Michael W. Oppenheimer, David B. Doman, and Kevin P. Bollino

DECEMBER 2006

Approved for public release; distribution unlimited.

STINFO COPY

AIR VEHICLES DIRECTORATE
AIR FORCE MATERIEL COMMAND
AIR FORCE RESEARCH LABORATORY
WRIGHT-PATTERSON AIR FORCE BASE, OH 45433-7542

NOTICE AND SIGNATURE PAGE

AFRL-VA-WP-TP-2007-303 HAS BEEN REVIEWED AND IS APPROVED FOR PUBLICATION IN ACCORDANCE WITH ASSIGNED DISTRIBUTION STATEMENT.

*//Signature//

Michael W. Oppenheimer
Electronics Engineer
Control Design and Analysis Branch
Air Force Research Laboratory
Air Vehicles Directorate

//Signature//

Deborah S. Grismer
Chief
Control Design and Analysis Branch
Air Force Research Laboratory
Air Vehicles Directorate

//Signature//

JEFFREY C. TROMP
Senior Technical Advisor
Control Sciences Division
Air Vehicles Directorate

This report is published in the interest of scientific and technical information exchange, and its publication does not constitute the Government's approval or disapproval of its ideas or findings.

*Disseminated copies will show "//Signature//" stamped or typed above the signature blocks.

REPORT DOCUMENTATION PAGE

Form Approved
OMB No. 0704-0188

1. REPORT DATE *(DD-MM-YY)*	2. REPORT TYPE	3. DATES COVERED *(From - To)*
December 2006	Journal Article Preprint	06/01/2004 – 12/18/2006

4. TITLE AND SUBTITLE
FAULT TOLERANT OPTIMAL TRAJECTORY GENERATION FOR REUSABLE LAUNCH VEHICLES (PREPRINT)

5a. CONTRACT NUMBER
In-house

5b. GRANT NUMBER

5c. PROGRAM ELEMENT NUMBER
62201F

6. AUTHOR(S)
Patrick J. Shaffer, I. Michael Ross, and Kevin P. Bollino (Naval Postgraduate School)
Michael W. Oppenheimer and David B. Doman (AFRL/VACA)

5d. PROJECT NUMBER
A03G

5e. TASK NUMBER

5f. WORK UNIT NUMBER
0B

7. PERFORMING ORGANIZATION NAME(S) AND ADDRESS(ES)

Naval Postgraduate School
Monterey, CA 93943

Control Design and Analysis Branch (AFRL/VACA)
Control Sciences Division
Air Vehicles Directorate
Air Force Materiel Command, Air Force Research Laboratory
Wright-Patterson Air Force Base, OH 45433-7542

8. PERFORMING ORGANIZATION REPORT NUMBER
AFRL-VA-WP-TP-2007-303

9. SPONSORING/MONITORING AGENCY NAME(S) AND ADDRESS(ES)

Air Vehicles Directorate
Air Force Research Laboratory
Air Force Materiel Command
Wright-Patterson Air Force Base, OH 45433-7542

10. SPONSORING/MONITORING AGENCY ACRONYM(S)
AFRL-VA-WP

11. SPONSORING/MONITORING AGENCY REPORT NUMBER(S)
AFRL-VA-WP-TP-2007-303

12. DISTRIBUTION/AVAILABILITY STATEMENT
Approved for public release; distribution unlimited.

13. SUPPLEMENTARY NOTES
Journal article submitted to Guidance, Control and Dynamics, published by AIAA.

14. ABSTRACT

Reconfigurable inner-loop control laws improve the fault tolerance of a vehicle to control effector failures; however, in order to preserve stability, the unfailed effectors may be deployed to off-nominal positions to compensate for undesirable perturbations caused by the failed effectors. The effectors acting under the influence of a reconfigurable control law can produce significant perturbations to the nominal forces produced by the wing and body and can also affect the range of flight conditions over which the vehicle can be controlled. Three degree-of-freedom (3 DOF) dynamical models used in trajectory optimization for aerospace vehicles typically include wing-body aerodynamic force effects but ignore the aerodynamic forces produced by the control surfaces. In this work, a method for including these trim effects as well as control induced trajectory constraints in a 3 DOF model is presented.

15. SUBJECT TERMS
Reconfigurable Control, Nonlinear Control Allocation, Trajectory Reshaping

16. SECURITY CLASSIFICATION OF:			17. LIMITATION OF ABSTRACT:	18. NUMBER OF PAGES	19a. NAME OF RESPONSIBLE PERSON (Monitor)
a. REPORT	b. ABSTRACT	c. THIS PAGE			Michael W. Oppenheimer
Unclassified	Unclassified	Unclassified	SAR	42	19b. TELEPHONE NUMBER *(Include Area Code)* N/A

Standard Form 298 (Rev. 8-98)
Prescribed by ANSI Std. Z39-18

Fault Tolerant Optimal Trajectory Generation for Reusable Launch Vehicles

Patrick J. Shaffer *

I. Michael Ross †

Michael W. Oppenheimer ‡

David B. Doman §

Kevin P. Bollino ¶

Reconfigurable inner-loop control laws improve the fault tolerance of a vehicle to control effector failures; however, in order to preserve stability, the unfailed effectors may be deployed to off-nominal positions to compensate for undesirable perturbations caused by the failed effectors. The effectors acting under the influence of a reconfigurable control law can produce significant perturbations to the nominal forces produced by the wing and body and can also affect the range of flight conditions over which the vehicle can be controlled. Three-degree-of-freedom (3 DOF) dynamical models used in trajectory optimization for aerospace vehicles typically include wing-body aerodynamic force effects but ignore the aerodynamic forces produced by the control surfaces. These so-called trim effects are a normal component of six-degree-of-freedom models; however, such models have been considered to be excessively cumbersome for the purposes of trajectory optimization. In this work, a method for including these trim effects as well as control induced trajectory constraints in a 3 DOF model is presented. The method makes use of nonlinear control allocation methods to determine the control effector positions required to rotationally balance the vehicle at each point in the flight envelope and uses that information to compute force perturbations and new control induced trajectory constraints. The method estimates the steady state response of a reconfigurable inner-loop control law by solving for the control surface deflections required to achieve rotational equilibrium over a range of flight conditions. This is accomplished by

*CDR, United States Navy, Naval Postgraduate School, Monterey, CA 93943

†Professor, Department of Mechanical and Astronautical Engineering, Naval Postgraduate School, Monterey, CA 93943, Email: imross@nps.edu. Associate Fellow, AIAA

‡Electronics Engineer, Control Design and Analysis Branch, 2210 Eighth Street, Ste 21, Air Force Research Laboratory, WPAFB, OH 45433-7531, Email Michael.Oppenheimer@wpafb.af.mil, Ph. (937) 255-8490, Fax (937) 656-4000, Member AIAA

§Senior Aerospace Engineer, Control Design and Analysis Branch, 2210 Eighth Street, Ste 21, Air Force Research Laboratory, WPAFB, OH 45433-7531 Email David.Doman@wpafb.af.mil, Ph. (937) 255-8451, Fax (937) 656-4000, Associate Fellow AIAA

¶Captain, United States Air Force, Naval Postgraduate School, Monterey, CA 93943, Email: kpbollin@nps.edu

passing knowledge of surface failures to a nonlinear control allocation algorithm in order to estimate the control surface deflections required to balance the vehicle. Upon solving for the required control surface deflections, the contributions of the control effectors to the vehicle lift and drag are computed, as well as 3 DOF compatible constraints that define regions of the flight envelope where the vehicle does not have sufficient control power to rotationally balance the vehicle. An example is presented that includes control failure effects in a maximum downrange trajectory optimization problem for the flight of an unpowered reusable launch vehicle passing through the atmosphere. Constrained trajectories are planned by solving the resulting optimal control problem using a Legendre pseudospectral method. State dependent constraints resulting from a control failure are included in the nonlinear optimal control problem. With accurate knowledge of the available maneuverability envelope and aerodynamics of the failed vehicle, it is demonstrated that the methods hold the potential to significantly enhance safety margins even when control effectors have failed.

Introduction

Autonomous reusable launch vehicles (RLV) are being pursued as low-cost alternatives to expendable launch vehicles and the Shuttle. The employment of autonomous, reusable launch vehicles requires additional robustness in guidance and control to fulfill the role of an adaptive human pilot in the event of failures or unanticipated conditions. Hence, new guidance strategies that are able to identify and adapt to vehicle failures during the flight and still safely return the vehicle to earth are required.[1] New advanced guidance and control algorithms (AG&C) have been developed that adapt and attempt to recover vehicles that have suffered failures or damage. A survey of historical launch vehicle failures that resulted in vehicle loss or degraded mission capabilities concluded that AG&C methods could improve mission performance or recover a reusable launch vehicle that experienced a similar failure.[2]

In this work, the framework for computing optimal trajectories for a nominal and failed vehicle is developed. The method presented here is designed to be used in conjunction with reconfigurable inner-loop flight control laws. While such control methods improve the fault tolerance of a vehicle to control effector failures; the unfailed effectors may be deployed in unusual ways to compensate for undesirable perturbations caused by the failed effectors. Reconfigurable control laws can therefore produce significant perturbations to the nominal forces produced by the wing and body and can also affect the range of flight conditions over which the vehicle can be controlled. Three-degree-of-freedom (3 DOF) dynamical models used in trajectory optimization for aerospace vehicles typically include wing-body aerodynamic force effects but ignore the aerodynamic forces produced by the control surfaces. These so-called trim effects are a normal component of six-degree-of-freedom models; however, such

models have historically been considered less attractive than 3 DOF models for the purposes of trajectory optimization. A method for including trim effects as well as control induced trajectory constraints in a 3 DOF model is presented. The method makes use of recent advances in nonlinear control allocation methods to determine the control effector positions required to rotationally balance the vehicle at each point in the flight envelope and uses that information to compute force perturbations and new control induced trajectory constraints. The method estimates the steady state response of a reconfigurable inner-loop control law by solving for the control surface deflections required to achieve rotational equilibrium over a range of flight conditions. This is accomplished by passing knowledge of surface failures to a nonlinear control allocation algorithm in order to estimate the control surface deflections required to balance the vehicle. Upon solving for the required control surface deflections, the contributions of the control effectors to the vehicle lift and drag are computed, as well as 3 DOF compatible constraints that define regions of the flight envelope where the vehicle does not have sufficient control power to rotationally balance the vehicle. Such constraints are state dependent and are utilized in an optimal control problem to replan trajectories that avoid regions of the flight envelope where the vehicle cannot maintain rotational equilibrium.

Trajectory and abort planning functions use a variety of optimality criteria as implicit requirements. For example, in abort planning for unpowered re-entry vehicles, the size of the footprint or reachable region on the surface of the earth is an important factor to consider. Maximizing vehicle footprint under failure conditions is important in order to allow one to select from as many landing sites as possible during exigency operations. Other trajectory generation and guidance problems include ascent, re-entry, terminal area energy management and approach and landing. Mease, et.al.,[3] developed a three dimensional entry trajectory planning method. Shen and Lu[4] develop a methodology to design 3 DOF entry trajectories and also describe a new automated lateral guidance logic based on crossrange.[5] Some of these methods focus on designing reference trajectories on-board in order to improve performance.[3,4,6,7] While these studies did not directly account for the effects of control effector failures and reconfigurable control system response, these methods could conceivably make use of the methods developed in this work that update the 3 DOF aerodynamic model to include trim force effects and flight envelope constraints. Related work has been accomplished that integrates adaptive guidance and control methods with trajectory modification methods to automatically respond to failures[8,23] and design abort trajectories online.[9]

For the purpose of illustrating the method of incorporating control surface failure effects into a 3 DOF aerodynamic model and estimating control failure induced flight envelope constraints, we consider the problem of determining the maximum downrange capability for an unpowered RLV under nominal and failed conditions. Under failure conditions, the safety

margins of traditional feedback control laws can diminish because they are not tuned for the failed vehicle or because they are based on inadequate dynamical models.[10] Oversimplified dynamical models that do not exploit the full maneuverability envelope of the vehicle can compromise safety.[11] By incorporating the forces produced by the control effectors into the 3 DOF models used for trajectory optimization, one can reduce aerodynamic model inaccuracies and estimate regions in the flight envelope that should be avoided due to a lack of control power and the inability to maintain rotational equilibrium at critical points in the flight envelope. Therefore, determining optimal trajectories under failure conditions is critical to safety. For example, a conventional footprint generation algorithm may incorrectly assess the feasibility of reaching a critical landing site, while a more sophisticated algorithm could generate revised optimal trajectories based on accurate failure effect information in order to safely recover a vehicle at a feasible landing site.[12] Thus, failure to perform trajectory optimization using accurate aerodynamic models and flight envelope constraint estimates for the failed vehicle could lead to incorrect conclusions regarding landing site feasibility during online abort planning.

The class of failures considered in this work are control surface failures whose effects can be described using the nominal aerodynamic database. Nominal trajectories are not necessarily feasible following a control surface failure. The challenge is to reconfigure the inner-loop control system to use the healthy control effectors to compensate for the undesired effects of the failed control effector and to replan a new trajectory based upon aerodynamic data, that includes off-nominal trim effects, to achieve an acceptable end condition. Despite the fact that this is an extremely difficult problem, recent research on pseudospectral (PS) methods for optimal control indicates that solving such problems are indeed within reach.[13,14] In this paper, we describe preliminary steps in achieving this ultimate goal.

This work builds upon the recent research of Fahroo and Doman[12] in demonstrating the application of a PS method to determine optimal trajectories for an RLV for nominal conditions as well as for off-nominal conditions caused by vehicle control surface failures. To this end, this paper integrates several different aspects of the guidance and control problem. X-33 vehicle aerodynamic data[15] is used in a 3 DOF dynamical model to generate the trajectories. The main thrust of this work is the inclusion of state-dependent Mach and angle of attack constraints in the optimization problem. These constraints are computed by forming a trim deficiency map, which displays regions in the Mach-angle of attack space where the vehicle can be rotationally trimmed. The boundary of the trimmable region is used as a constraint in the optimization problem, requiring that any reshaped trajectories lie in the trimmable region. The example utilized here is the problem of determining the maximum downrange for a footprint analysis. Heating and dynamic pressure constraints

are not included in the optimization problem (normal force is included), however, these can be easily incorporated with the framework presented here. In essence, the work presented here is general and can accommodate a wide range of trajectory problems. With suitable modifications to the optimization problem (changes to the cost and constraints), entry and approach and landing guidance problems and heating and dynamic pressure constraints can be considered.

Constructing the Dynamical Model: Motivation and Issues

For guidance purposes, it is common practice to consider a 3 DOF model that describes the point-mass motion. The angle of attack, α, and bank angle, σ, are selected to be the control inputs. A 3 DOF model for flight over a flat earth is given by:[16]

$$\dot{x} = V\cos\chi\cos\gamma \tag{1}$$

$$\dot{y} = V\sin\chi\cos\gamma \tag{2}$$

$$\dot{z} = V\sin\gamma \tag{3}$$

$$\dot{V} = -\frac{C_D(M,\alpha)A_{ref}\rho V^2}{2m} - g\sin\gamma \tag{4}$$

$$\dot{\gamma} = \frac{C_L(M,\alpha)A_{ref}\rho V\cos\sigma}{2m} - \frac{g\cos\gamma}{V} \tag{5}$$

$$\dot{\chi} = \frac{C_L(M,\alpha)A_{ref}\rho V\sin\sigma}{2m} \tag{6}$$

where x (down range), y (cross-range), and z (altitude) are the vehicle's position, γ is the flight path angle, χ is the azimuth angle, σ is the bank angle, V is the velocity magnitude, ρ is the freestream mass density, A_{ref} is a characteristic area for the body, and C_L and C_D are the lift and drag coefficient functions that depend upon the Mach number, M, and angle of attack, α.

In order to ensure smoothness of the controls $\alpha(\cdot)$ and $\sigma(\cdot)$, we define the rates $\dot{\alpha}(\cdot)$ and $\dot{\sigma}(\cdot)$ as the control inputs and add two additional states to the 3 DOF equations of motion:

$$\dot{\alpha}(t) \triangleq u_\alpha(t) \tag{7}$$

$$\dot{\sigma}(t) \triangleq u_\sigma(t) \tag{8}$$

where $\mathbf{u} := (u_\alpha, u_\sigma) \in \mathbb{R}^2$ are the controls that must be selected from some compact set, $\mathbb{U} \subset \mathbb{R}^2$. In this work, we use

$$\mathbb{U} := \{(u_\alpha, u_\sigma) : \ |u_\alpha| \leq 40\ deg/s, \quad |u_\sigma| \leq 40\ deg/s\} \tag{9}$$

It is worth noting that in the absence of this specification, $\alpha(\cdot)$ and $\sigma(\cdot)$ may exhibit highly dynamic behavior depending upon the type of guidance problem.[15,17] Thus, by adding these rate dynamics to the 3 DOF model, we arrive at an eight dimensional state vector, that is, $\mathbf{x} \in \mathbb{R}^8$.

The vehicle lift and drag coefficients, C_L and C_D, are functions of Mach number and angle of attack and can be broken down into a component from the base or wing-body and increments due to the deflection of aerodynamic control surfaces:[15]

$$\begin{aligned} C_L\left(M,\alpha\right) &= C_{L_o}\left(M,\alpha\right) + C_{L_{\delta^*}}\left(M,\alpha,\boldsymbol{\delta}^*(M,\alpha)\right) \\ C_D\left(M,\alpha\right) &= C_{D_o}\left(M,\alpha\right) + C_{D_{\delta^*}}\left(M,\alpha,\boldsymbol{\delta}^*(M,\alpha)\right) \end{aligned} \tag{10}$$

where $(M,\alpha) \mapsto (C_{L_0}, C_{D_0})$ are based upon static table-look up data while $(M,\alpha) \mapsto (C_{L_{\delta^*}}, C_{D_{\delta^*}})$ are based upon an algorithmic map, $(M,\alpha) \mapsto \boldsymbol{\delta}^*$, and $\boldsymbol{\delta}^*$ is a solution to a control allocation algorithm used to trim the vehicle. The quantities, $C_{L_o}\left(M,\alpha\right)$ and $C_{D_o}\left(M,\alpha\right)$ are base lift and drag coefficients, while $C_{L_{\delta^*}}\left(M,\alpha,\boldsymbol{\delta}^*(M,\alpha)\right)$ and $C_{D_{\delta^*}}\left(M,\alpha,\boldsymbol{\delta}^*(M,\alpha)\right)$ are the control induced lift and drag increments. The quantity $\boldsymbol{\delta} = \boldsymbol{\delta}^*$ corresponds to a trim vector of inner-loop control variables that establish rotational equilibrium at a given flight condition. Nominally, there exist 8 aerodynamic control surfaces on the X-33: left and right rudders, body flaps, inboard and outboard elevons. The X-33 is shown in Fig. 1. These control surface deflection variables, collectively known as the effector vector, are given by

$$\boldsymbol{\delta} = \left[\; \mathit{Elevon}_{R_I},\; \mathit{Elevon}_{R_O},\; \mathit{Elevon}_{L_I},\; \mathit{Elevon}_{L_O},\; \mathit{Flap}_R,\; \mathit{Flap}_L,\; \mathit{Rudder}_R,\; \mathit{Rudder}_L \;\right]^T \tag{11}$$

In Eq. 11, the subscripts are defined as R_I=right inboard, R_O=right outboard, L_I=left inboard, L_O=left outboard, R=right, and L=left. The trim control deflection vector $\boldsymbol{\delta}^*$ is obtained by solving a nonlinear control allocation problem that enforces actuator limits and accommodates locked or floating aerodynamic surface failures.

It should be noted that in this exposition, the effect of sideslip angle on the lift and drag forces is ignored for the sake of clarity. Adding a third independent variable would result in four-dimensional trim constraint regions, which would be difficult to view and analyze. This manuscript considers failures for which there exists sufficient control power to maintain zero sideslip angle. Nevertheless, the methods presented here are general in that flight at non-zero sideslip conditions can be accommodated; however, the lift, drag, and moment coefficients become functions of Mach, angle of attack, and sideslip thereby making visualization of trim maps difficult.

Control Allocation in Failure Modes

The RLV control surfaces are position limited and have maximum and minimum deflections. In this work, $\boldsymbol{\delta}$ is limited by

$$\begin{aligned} \boldsymbol{\delta}_{min} &= \left[\begin{array}{cccccccc} -30, & -30, & -30, & -30, & -15, & -15, & -60, & -30 \end{array} \right] \\ \boldsymbol{\delta}_{max} &= \left[\begin{array}{cccccccc} 30, & 30, & 30, & 30, & 26, & 26, & 30, & 60 \end{array} \right] \end{aligned} \tag{12}$$

where the numbers are in degrees. Numerous reconfigurable inner-loop control methods exist whose purpose is to maintain control of a vehicle (when physically possible) in the event of a failure or damage by using the healthy control surfaces to compensate for the effects of the failed surfaces.[1,8,18–22] Under some failure conditions, reconfigurable inner-loop control is insufficient to recover a vehicle that also relies on an autonomous guidance system that follows a prescribed trajectory.[23] Significant changes to the aerodynamics and a possible lack of control power may force one to determine a new trajectory based on knowledge of the effect of a failure. Failures may result in changes in the constraints on the state, cost, control, and path arguments that correspond to the problem of computing a new optimal trajectory for a failed vehicle. A replanned trajectory must be computed that provides the ability to complete a mission to a terminal objective in order to safely recover the vehicle. Traditional methods store the trajectory data for a limited set of pre-planned engine-out or control surface failure scenarios and therefore require significant pre-planning, forethought, and data storage for implementation. While data storage problems are beginning to disappear, conceiving all possible failure combinations and designing trajectories for each case is at best, a formidable and painstaking task. An appealing alternative is to develop a fault tolerant autonomous guidance, control, and trajectory shaping system that can be executed in-flight and respond to failures as they occur. In support of this goal, we describe the development of an online algorithm that can provide a trajectory reshaping algorithm with an updated aerodynamic database that accurately represents the effects of locked or floating aerodynamic surfaces, and provides a constraint map that describes the feasible range of Mach number and angle of attack for which the vehicle can be rotationally trimmed. Thus, the algorithm allows one to include 6 DOF trim effects and constraints in the 3 DOF dynamical model described earlier.

It is assumed that the vehicle has sufficient control authority to trim in symmetric flight (zero sideslip angle) and that the total lateral wing-body force and moment coefficients can be driven to zero. We also assume that the body-axis angular velocity vector is small such that damping derivative contributions to the vehicle moment are insignificant. Thus, the base moments for this study are functions of Mach number and angle of attack only. The necessary conditions to rotationally trim the vehicle are that the moments resulting from all

control surface deflections (failed and healthy) must be equal and opposite to the moments produced by the wing-body. Thus,

$$\begin{pmatrix} C_{rm_\delta}(M,\alpha,\boldsymbol{\delta}) \\ C_{m_\delta}(M,\alpha,\boldsymbol{\delta}) \\ C_{ym_\delta}(M,\alpha,\boldsymbol{\delta}) \end{pmatrix} = \begin{pmatrix} 0 \\ -C_{m_o}(M,\alpha) \\ 0 \end{pmatrix} \tag{13}$$

where $C_{rm_\delta}(M,\alpha,\boldsymbol{\delta})$, $C_{m_\delta}(M,\alpha,\boldsymbol{\delta})$, and $C_{ym_\delta}(M,\alpha,\boldsymbol{\delta})$ are the rolling, pitching, and yawing moment coefficients produced by the control effectors and $C_{m_o}(M,\alpha)$ is the wing-body pitching moment.

A nonlinear control allocation algorithm[24] is used to determine the effector displacement vector that satisfies Eq. 13 and attempts to simultaneously minimize the 1-norm of the displacement vector. This vector is nominally subject to the limits of Eq. 12 or by a modified set of position limits that reflect the current health of the effector suite. The control allocation problem uses an iterative algorithm[25] that queries the full 6 DOF aerodynamic database. The constrained control allocation problem is given by:

$$\min_{\boldsymbol{\delta}} J_D = \min_{\boldsymbol{\delta}} \left\| \begin{bmatrix} 0 \\ -C_{m_{oj,i}}(M_j,\alpha_i) \\ 0 \end{bmatrix} - \begin{bmatrix} C_{rm_{\delta j,i}}(M_j,\alpha_i,\boldsymbol{\delta}_{j,i}) \\ C_{m_{\delta j,i}}(M_j,\alpha_i,\boldsymbol{\delta}_{j,i}) \\ C_{ym_{\delta j,i}}(M_j,\alpha_i,\boldsymbol{\delta}_{j,i}) \end{bmatrix} \right\|_1 \tag{14}$$

subject to

$$\boldsymbol{\delta}_{min} \leq \boldsymbol{\delta} \leq \boldsymbol{\delta}_{max} \tag{15}$$

at each Mach-α point in the aerodynamic database. Notice that the upper and lower bounds on $\boldsymbol{\delta}$ are dependent on the operating mode of the vehicle. A vehicle operating under nominal conditions has the full range of deflections available, while a vehicle operating with a control surface failure has a subset of the nominal displacement vector's range. A nonzero value for Eq. 14 means that there is insufficient control power to rotationally trim the vehicle (it is trim deficient), and that the vehicle would be at risk of departing controlled flight at that particular flight condition. The trim deficient regions in Mach-α space can be mapped and identified as flight envelope boundaries that constrain the trajectory. If the control allocation algorithm is able to rotationally trim the vehicle, any excess control power can be used to maneuver the vehicle. The control allocator employs a second control allocation optimization algorithm to minimize the deviation from a minimum control deflection condition. This condition is represented by an eight-element preference vector set to zero and roughly

corresponds to a minimum drag condition. The second optimization is

$$\min_{\boldsymbol{\delta}} J_S = \min_{\boldsymbol{\delta}} \left\| \mathbf{W} \left(\boldsymbol{\delta} - \boldsymbol{\delta}_p \right) \right\|_1 \tag{16}$$

subject to

$$\boldsymbol{\delta}_{min} \leq \boldsymbol{\delta} \leq \boldsymbol{\delta}_{max} \tag{17}$$

and

$$\begin{pmatrix} C_{rm_\delta}(M, \alpha, \boldsymbol{\delta}) \\ C_{m_\delta}(M, \alpha, \boldsymbol{\delta}) \\ C_{ym_\delta}(M, \alpha, \boldsymbol{\delta}) \end{pmatrix} = \begin{pmatrix} 0 \\ -C_{m_o}(M, \alpha) \\ 0 \end{pmatrix} \tag{18}$$

In Eq. 16, $\mathbf{W}$ is a weighting matrix used to weight the importance of driving an effector to its preferred location. In the case where the vehicle is operating with excess control power, the effector displacement vector is the output of the second optimization routine, otherwise $\boldsymbol{\delta}$ minimizes the trim deficiency. Here we set the preference vector $\boldsymbol{\delta}_p = \mathbf{0}$ since this roughly corresponds to minimizing control effector drag which is compatible with the higher level objective of maximizing downrange. The effector displacement vector that is the solution to the control allocation problem is represented as $\boldsymbol{\delta}^*$ to delineate it from the possibly multiple combinations of control surface deflections that are available to achieve the same desired control but are not optimized for minimum control deflection.

It is important that a nonlinear control allocation algorithm be used to solve for the deflection vector because the moments are nonlinear functions of control surface deflection. While linear methods may be suitable for inner-loop flight control applications, they fail to capture the global character of nonlinear moment-deflection curves and may lead to erroneous trim deflection vectors that fail to trim the vehicle. The piecewise linear control allocation method of Bolender[24] was used in this case and has been found to yield acceptable results for cases involving separable nonlinearities.

Incorporating Trim Deficiency Maps In Trajectory Replanning

The vehicle is assumed to operate in the nominal condition until a failure has been identified through an online fault detection or identification algorithm, at which point a new lift and drag table corresponding to the failed vehicle configuration is generated. Once a failure has been identified, the control allocator generates a new set of control deflections for the failed vehicle and uses the aerodynamic database to determine the new trim lift and drag contributions. In the process of computing the control deflections for the failed vehicle, points in the Mach-α envelope for which the vehicle cannot be trimmed are identified.

These trim deficiency regions must be avoided and are thus used as path constraints for the trajectory replanning. A point in the Mach-α space is called trim deficient if no control effector vector, $\boldsymbol{\delta}$, can be found to identically satisfy Eq. 13. The aerodynamic data table is then changed to account for the current failed condition and a new trajectory is generated for the new aerodynamics and path constraints. Figures 2 and 3 show the trim deficiency maps for a nominal case and a case of both bodyflaps failed at 26°. In three-dimensions, Fig. 3 becomes the plot shown in Fig. 4. Notice, from Fig. 2, that the maximum trim deficiency value is on the order of machine precision so that the entire range of combinations of angles of attack and Mach numbers is considered to be available in the nominal (unfailed) case. Hence, the unfailed vehicle can be trimmed over the entire Mach-α space. When the bodyflaps are locked at 26°, the envelope describing allowable Mach numbers-angles of attack is now severely reduced (see Figs. 3 and 4). Points in the Mach-α envelope where the pitch deficiency is non-zero indicate that there is insufficient control power to rotationally balance the vehicle and that vehicle control would be in jeopardy at such conditions. This establishes a restricted region that, if possible, feasible trajectories should avoid. Ideally, the trajectory will have a clear path in Mach-α space from the initial conditions to the final conditions. A clear path is defined as a path from one point defined by the flight condition (Mach-α) to another point (Mach-α) with no intervening regions of unacceptable trim deficiency. Should a path cross into or through a region of pitch deficiency, the trajectory is declared infeasible because the vehicle cannot be rotationally balanced over part of the candidate trajectory. Failure conditions can result in situations where no clear path exists. In such cases, one might select a path where the least severe moment deficiency is encountered.

Having obtained the control effector settings that rotationally balance the vehicle, the total lift and drag acting on the vehicle can be computed. Utilizing $\boldsymbol{\delta}^*(M, \alpha)$ from the control allocation problem, the aerodynamic database can be queried to determine the control surface induced lift and drag contributions. Figures 5 and 6 show the nominal and failed lift and drag maps over the entire Mach-α range of interest. In this case, the failure of the bodyflaps at 26° does not significantly affect the lift of the vehicle, however, large changes are seen in the drag. The constraint boundary and updated lift and drag maps are made available to a trajectory reshaping algorithm to ensure that a feasible trajectory, if one exists, is computed.

The algorithm to compute pitch deficiency, lift, and drag maps and to determine the range of trimmable angle of attack is summarized as follows:[25]

1. Define a grid for Mach and Angle of Attack, including lower and upper bounds and step size

2. Initialize $\boldsymbol{\delta}$

3. Loop 1 → For j = 1 to Number of Machs
4. Loop 2 → For i = 1 to Number of Angles of Attack
5. Compute the wing-body pitching moment coefficient, $C_{m_{oj,i}}(M_j, \alpha_i)$
6. Solve a control allocation problem to find $\boldsymbol{\delta}^*_{j,i}$ which satisfies Eq. 13
7. Compute trim deficiency at each point, i.e., deficiency(j,i) = $\left\| \begin{bmatrix} 0 \\ -C_{m_{oj,i}}(M_j, \alpha_i) \\ 0 \end{bmatrix} - \begin{bmatrix} C_{rm_{\delta j,i}}(M_j, \alpha_i, \boldsymbol{\delta}_{j,i}) \\ C_{m_{\delta j,i}}(M_j, \alpha_i, \boldsymbol{\delta}_{j,i}) \\ C_{ym_{\delta j,i}}(M_j, \alpha_i, \boldsymbol{\delta}_{j,i}) \end{bmatrix} \right\|_2$
8. If deficiency(j,i) = 0, the vehicle can be trimmed at the corresponding Mach-α combination
9. Compute drag and lift at each data point by substituting $\boldsymbol{\delta}^*_{j,i}$ into the aerodynamic database
10. Increment Mach and/or Alpha
11. End Angle of Attack loop
12. End Mach loop

This algorithm yields the control deficiency map as well as the lift and drag maps. Each map is valid for all operating conditions for which a model is available.

Note that the previous discussion does not consider any other limitations such as normal force, heating, or dynamic pressure on the trajectory. These constraints may further reduce the area available for a feasible trajectory and can be taken into account when solving the optimal control problem by appending additional inequality constraints. It is possible that, in some cases, these additional constraints will completely eliminate a clear path. It is easier to visualize the optimal trajectory with constraints as a region through Mach-α space for which the vehicle can be rotationally trimmed without violating normal force, heating, or dynamic pressure constraints. If a failure causes this corridor to close, a clear path to the end mission may not exist. Therefore, feasible trajectories are not available and flight termination may be the only option.

Trajectory Replanning Optimal Control Problems

A typical trajectory computation problem considers a vehicle, at some initial position, and seeks to generate an optimal trajectory that brings it to a final state specified by an endpoint condition, subject to constraints. The resulting optimal trajectory minimizes some performance index, which can include some function of the vehicle states and/or control inputs. Typical performance indices are maximizing downrange, maximizing cross range, minimizing control effort, or some weighted combination of these indices. In this section, we illustrate how to incorporate the effects of control failures, using the methods discussed in the previous sections, into the solution of a maximum downrange problem for an unpowered RLV.

As discussed in the previous sections, a 3 DOF dynamic model, that incorporates information derived from a 6 DOF model, will be used. In particular, we incorporate the effects of aerodynamic surface induced lift and drag from a high-fidelity aerodynamic database and we determine the region in Mach-α space over which rotational equilibrium can be achieved. In order to determine a trajectory that maximizes downrange, we select the following cost function:

$$J[\mathbf{x}(\cdot), \mathbf{u}(\cdot), t_0, t_f] := -x(t_f) \tag{19}$$

where the elements of $\mathbf{x}$ are given by,

$$\mathbf{x} = \left[\begin{array}{cccccccc} x & y & z & M & \gamma & \chi & \alpha & \sigma \end{array} \right]^T \tag{20}$$

The initial conditions for the example mission are

$$\mathbf{x}_i = \begin{pmatrix} x_i \\ y_i \\ z_i \\ M_i \\ \gamma_i \\ \chi_i \\ \alpha_i \\ \sigma_i \end{pmatrix} = \begin{pmatrix} 0 \\ 0 \\ 125,000 ft \\ 8 \\ -1.3^\circ \\ 0 \\ 0 \\ 0 \end{pmatrix} \tag{21}$$

The target set, $\mathbb{E}_f$, is defined in terms of functional inequalities,

$$\mathbb{E}_f := \left\{ (\mathbf{x}_f, t_f) \in \mathbb{R}^8 \times \mathbb{R} : \ \mathbf{e}_f^L \leq \mathbf{e}_f(\mathbf{x}_f, t_f) \leq \mathbf{e}_f^U \right\} \tag{22}$$

where,

$$\mathbf{e}_f(\mathbf{x}_f, t_f) = \begin{bmatrix} z_f \\ M_f \\ V_f \sin\gamma_f \end{bmatrix} \tag{23}$$

and $\mathbf{e}_f^L$ and $\mathbf{e}_f^U$ are lower and upper bounds on the values of the function $\mathbf{e}_f$, given by

$$\mathbf{e}_f^L = \begin{bmatrix} 500 \ \ ft \\ 0.147 \\ -1500\frac{ft}{min} \end{bmatrix} \qquad \mathbf{e}_f^U = \begin{bmatrix} 500 \ \ ft \\ 0.153 \\ 500\frac{ft}{min} \end{bmatrix} \tag{24}$$

This target set is representative of desired conditions on approach to landing. In this example, the final angles of attack and bank are not specified. Should the vehicle arrive at the target set in an unrecoverable position (high angles of attack and bank along with large vertical speed) these variables as well as their associated acceptable range of values at the end point can easily be incorporated in the definition of $\mathbb{E}_f$.

Path constraints are derived primarily from the design and mission considerations of the vehicle and can be written as

$$\begin{bmatrix} -3g \\ -\infty \end{bmatrix} \leq \begin{bmatrix} n_z \\ J_D \end{bmatrix} \leq \begin{bmatrix} 6g \\ 0 \end{bmatrix} \tag{25}$$

where J_D is defined in Eq. 14. Equation 25 places a constraint on normal force and additionally constrains the vehicle's path to reside in a location in Mach-α space where the vehicle can be rotationally trimmed.

The state constraints are given by

$$\begin{bmatrix} -\infty ft \\ -\infty ft \\ 0ft \\ 0 \\ -\frac{\pi}{2}rad \\ -\infty rad \\ -10^\circ \\ -1^\circ \end{bmatrix} \leq \begin{pmatrix} x \\ y \\ z \\ M \\ \gamma \\ \chi \\ \alpha \\ \sigma \end{pmatrix} \leq \begin{bmatrix} \infty ft \\ \infty ft \\ \infty ft \\ \infty \\ \frac{\pi}{2}rad \\ \infty rad \\ 50^\circ \\ 1^\circ \end{bmatrix} \tag{26}$$

It is now apparent that once the problem has been formulated, it can be posed as a

constrained, nonlinear optimal control problem of the following type:

$$(\mathsf{B}) \begin{cases} \mathsf{Minimize} & J[\mathbf{x}(\cdot), \mathbf{u}(\cdot), t_0, t_f] \\ \mathsf{Subject\ to} & \dot{\mathbf{x}}(t) = \mathbf{f}(\mathbf{x}(t), \mathbf{u}(t), t) \\ & \mathbf{u}(t) \in \mathbb{U}(t, \mathbf{x}(t)) \\ & \mathbf{x}(t) \in \mathbb{X}(t) \\ & (\mathbf{x}(t_0), \mathbf{x}(t_f), t_0, t_f) \in \mathbb{E} \end{cases}$$

where $\mathbb{U}$ is written in a form to indicate state-dependent control constraints. Since solving optimal control problems, particularly state-constrained problems, are widely considered to be difficult,[26,27] it is no surprise that these problems belong to the class of difficult problems. Nonetheless, over the last decade there has been substantial progress in solving optimal control problems. Surprisingly, much of this progress can be attributed to a new understanding of the fundamental issues of solving optimal control problems.[27–32] In order to solve the optimal control problem, the software package DIDO is utilized.[33]

One last point concerning the trajectories computed in this work is that these trajectories are open-loop. The idea behind this work is to be able to incorporate the 6 DOF effects of failures online to compute new feasible trajectories. This work provides a step towards solving the problem of including 6 DOF effects in trajectory replanning algorithms. Even though closed-loop trajectories computed online has not been the focus of this effort, it is envisioned that the work presented here could be modified for closed-loop guidance.

Results

The following section discusses solutions to the maximum downrange problem under nominal conditions and in the presence of a control failure. As discussed in the previous sections, we analyze a control failure condition where the bodyflaps become locked at 26°, which is a case that alters the control surface induced lift and drag and also places significant constraints on the flight envelope. The trajectories for both the failed and nominal vehicles start at the initial conditions described in Eq. 21 and satisfy the constraints of Eq. 25. The initial conditions correspond to a point in the flight envelope where the vehicle makes use of its aerodynamic control surfaces to control the trajectory. The vehicle experiencing a control surface failure must observe the trim deficiency path constraint, while the nominal vehicle is unconstrained by trim deficiency because, as shown in Fig. 2, the vehicle has adequate control power to trim over the entire flight envelope.

The downrange profiles for both trajectories are shown in Fig. 7. As expected, the downrange for the nominal vehicle is much larger than the downrange for the failed vehicle. For the bodyflaps locked at 26°, a severe drag penalty is imposed, hence, limiting the downrange.

Figures 8 and 9 display the altitude and velocity profiles for the nominal and failed vehicles over the entire flight, while Figures 10 and 11 display the altitude and velocity profiles for only the end of the mission. The end mission requirements of 500 ft altitude and Mach between 0.147 and 0.153 are achieved. The final velocity is about $167.2\frac{ft}{sec}$ and the final altitude is 500 ft. The last endpoint condition, from Eq. 24, to be met is the sink rate, which is a function of flight path angle. Figure 12 shows the flight path angle profiles over the entire simulation run, while Fig. 13 displays the flight path angles near the end of the run. The flight path angles for these two trajectories differ as a consequence of the controls available to the individual vehicles. The failed vehicle exhibits a very steep descent but ends the trajectory with a similar terminal maneuver as the nominal trajectory. The similarity of the terminal maneuvers is a direct result of the endpoint conditions shared by the two trajectories. Computing the sink rates yield values of about $-9\frac{ft}{sec}$ for the nominal vehicle and $3\frac{ft}{sec}$ for the failed vehicle. Therefore, all desired endpoint conditions have been met and, while the time histories for all states are not shown, the state constraints are not violated.

The failed bodyflaps do produce significant aerodynamic changes. Physically, the nominal trajectory trades excess speed for altitude, as can be seen in Figs. 8 and 9. At the top of the zoom climb, the vehicle assumes the best lift/drag configuration. The trajectory for the vehicle with the locked bodyflaps is prevented from flying the same angle of attack profile as the nominal vehicle because of the trim deficiency constraint. The trajectory does use the largest allowable angle of attack but this is insufficient to produce the zoom climb observed in the nominal trajectory. This is more evident when comparing the angle of attack profiles, as shown in Fig. 14. The nominal constraints on angle of attack of -10° to 50° are clearly not violated and significant differences between the nominal and failed profiles exist. Notice that the angles of attack of the failed vehicle are small, due to the pitch deficiency constraint. When the speed of the failed vehicle is below about Mach = 0.4, the trim deficiency goes to zero for all angles of attack. Hence, even the failed vehicle can perform the flare maneuver shown in Fig. 14. Since this example is a maximum downrange case, the bank angle is approximately zero and within the $\pm 1^\circ$ constraint as shown in Fig. 15.

A novel aspect of this work is the inclusion of state-dependent constraints into the optimization problem, in particular, the trim deficiency maps. Recall that it is desired that the reshaped trajectory lie in a region in the Mach-α space where the vehicle can be rotationally trimmed, if physically possible. The restricted region in Mach-α space that results from consideration of moment trim deficiency for the vehicle with locked flaps, imposes severe trajectory performance penalties as shown in Figs. 3 and 4. Figure 16 shows the differences between the two trajectories in Mach-α space as well as providing visual verification that the trajectory for the vehicle experiencing flap failure does not violate the imposed trim

deficiency constraint of 0.003 and instead closely follows the contour in regions where the constraint is active. Finally, we note that there are a number of other issues in fault-tolerant trajectory optimization that are beyond the scope of the present paper; some of these issues are discussed by Shaffer.[15]

Conclusions

By integrating recent advances in solving optimal control problems with inner-loop control allocation, it has been shown that it is possible to generate new feasible trajectories for an air vehicle that has experienced control effector failures. Methods were developed that allow the effects of locked and floating aerodynamic control surface failures to be incorporated into 3 DOF models used for trajectory optimization. Once a failure has been identified, its effects on the ability of the vehicle to trim can be determined and a trim deficiency map can be constructed. For the cases investigated, the map is a function of Mach number and angle of attack. Since Mach number is a state variable (i.e. scaled version of speed), incorporating trim deficiency into the optimization problem generates a state-dependent control constraint. Although such problems are notoriously difficult to solve, results show that pseudospectral methods are capable of solving them. When the methods were applied to an example, it was shown that a locked control effector can have a significant impact upon the selection of an optimal trajectory and that attempting to fly a trajectory designed for the nominal vehicle would not be feasible. It was shown that by recomputing the trajectory using an aerodynamic database that accounted for control surface failure effects and new flight envelope constraints that arise as a result of the control surface failure, one can successfully generate trajectories that can enable vehicle recovery.

References

[1]Hanson, J., " A Plan for Advanced Guidance and Control Technology for 2nd Generation Reusable Launch Vehicles," *Proceedings of the 2002 Guidance, Navigation and Control Conference*, AIAA Paper No. 2002-4557, August 2002.

[2]Hanson, J. M., "New Guidance For New Launchers," March 2003.

[3]Mease, K. D., Chen, D. T., Teufel, P., and Schönenberger, H., "Reduced-Order Entry Trajectory Planning for Acceleration Guidance," *Journal of Guidance, Control, and Dynamics*, Vol. 25, No. 2, 2002, pp. 257–266.

[4]Shen, Z. and Lu, P., "Onboard Generation of Three-Dimensional Constrained Entry Trajectories," *Journal of Guidance, Control, and Dynamics*, Vol. 26, No. 1, 2003, pp. 111–121.

[5]Shen, Z. and Lu, P., "Dynamic Lateral Entry Guidance Logic," *Journal of Guidance, Control, and Dynamics*, Vol. 27, No. 6, 2004, pp. 949–959.

[6]Zimmerman, C., Dukeman, G., and Hanson, J., "An Automated Method to Compute Orbital Entry Re-Entry Trajectories with Heating Constraints," *Journal of Guidance, Control, and Dynamics*, Vol. 26, No. 4, 2003, pp. 523–529.

[7]Lu, P., Sun, H., and Tsai, B., "Closed-Loop Endoatmospheric Ascent Guidance," *Journal of Guidance, Control, and Dynamics*, Vol. 26, No. 2, 2003, pp. 283–294.

[8]Johnson, E. N., Calise, A. J., Curry, M. D., Mease, K. D., and Corban, J. E., "Adaptive Guidance and Control for Autonomous Hypersonic Vehicles," *Journal of Guidance, Control, and Dynamics*, Vol. 29, No. 3, 2006, pp. 725–737.

[9]Calise, A. J. and Brandt, N., "Generation of Launch Vehicle Abort Trajectories Using a Hybrid Optimization Method," *Journal of Guidance, Control, and Dynamics*, Vol. 27, No. 6, 2004, pp. 930–937.

[10]Fahroo, F., Doman, D., and Ngo, A., " Modeling Issues in Footprint Generation for Reusable Launch Vehicles," *Proceedings of the 2003 IEEE Aerospace Conference*, Vol. 6, March 2003.

[11]Fahroo, F., Doman, D., and Ngo, A., " Footprint Generation for Reusable Launch Vehicles Using a Direct Pseudospectral Method," *Proceedings of the American Control Conference*, June 2003.

[12]Fahroo, F. and Doman, D., " A Direct Method for Approach and Landing Trajectory Reshaping with Failure Effect Estimation," *Proceedings of the Guidance, Navigation, and Control Conference*, AIAA Paper 2004-4772, August 2004.

[13]Ross, I. M. and Fahroo, F., " A Unified Framework for Real-Time Optimal Control," *Proceedings of the IEEE Conference on Decision and Control*, December 2003.

[14]Ross, I. M. and Fahroo, F., "Issues in the Real-Time Computation of Optimal Control," *Mathematical and Computer Modelling*, Vol. 43, No. 9-10, 2006, pp. 1172–1188.

[15]Shaffer, P. J., *Optimal Trajectory Reconfiguration and Retargeting for the X-33 Reusable Launch Vehicle*, Master's thesis, Naval Post Graduate School, 2004.

[16]Wiesel, W. E., *Spaceflight Dynamics*, McGraw-Hill, New York, NY, 1989.

[17]Josselyn, S. and Ross, I. M., "Rapid Verification Method for the Trajectory Optimization of Reentry Vehicles," *Journal of Guidance, Control, and Dynamics*, Vol. 26, No. 3, 2003, pp. 505–508.

[18]Härkegård, O., " Dynamic Control Allocation Using Constrained Quadratic Programming," *Proceedings of the 2002 Guidance, Navigation and Control Conference*, AIAA Paper No. 2002-4761, August 2002.

[19]Buffington, J. M., " Modular Control Law Design for the Innovative Control Effectors (ICE) Tailless Fighter Aircraft Configuration 101-3," Tech. Rep. AFRL-VA-WP-TR-1999, Air Force Research Laboratory, Wright-Patterson A.F.B., OH, 1999, pp 93-94.

[20]Enns, D. F., " Control Allocation Approaches," *Proceedings of the 1998 Guidance, Navigation and Control Conference*, AIAA Paper No. 98-4109, August 1998.

[21]Bodson, M., "Evaluation of Optimization Methods for Control Allocation," *Proceedings of the 2001 Guidance, Navigation and Control Conference*, AIAA, August 2001.

[22]Durham, W., "Constrained Control Allocation: Three Moment Problem," *Journal of Guidance, Control and Dynamics*, Vol. 16, No. 4, 1993, pp. 717–725.

[23]Schierman, J. D., Ward, D. G., Hull, J. R., Gandhi, N., Oppenheimer, M. W., and Doman, D. B., "Integrated Adaptive Guidance and Control for Re-Entry Vehicles with Flight-Test Results," *Journal of Guidance, Control and Dynamics*, Vol. 27, No. 6, 2004, pp. 975–988.

[24]Bolender, M. A. and Doman, D. B., "Nonlinear Control Allocation Using Piecewise Linear Functions," *Journal of Guidance, Control, and Dynamics*, Vol. 27, No. 6, 2004, pp. 1017–1027.

[25]Oppenheimer, M., Doman, D., and Bolender, M., "A Method for Estimating Control Failure Effects for Aerodynamic Vehicle Trajectory Retargeting," *Proceedings of the 2004 AIAA Guidance, Navigation and Control Conference*, AIAA Paper No. 2004-5169, August 2004.

[26]Vinter, R. B., *Optimal Control*, Birkhäuser, Boston, MA, 2000.

[27]Hager, W. W., "Numerical Analysis in Optimal Control," *International Series of Numererical Mathematics*, Vol. 139, 2001, pp. 83–93.

[28]Hager, W. W., "Runge-Kutta Methods in Optimal Control and the Transformed Adjoint System," *Numerische Mathematik*, Vol. 87, 2000, pp. 247–282.

[29]Betts, J. T., Biehn, N., and Campbell, S. L., "Convergence of Nonconvergent IRK Discretizations of Optimal Control Problems with State Inequality Constraints," *SIAM Journal of Scientific Computing*, Vol. 23, No. 6, 2002, pp. 1981–2007.

[30]Ross, I. M., "A Roadmap for Optimal Control: The Right Way to Commute," *Annals of the New York Academy of Sciences*, Vol. 1065, 2006.

[31]Mordukhovich, B. S., *Variational Analysis and Generalized Differentiation, I: Basic Theory*, Springer, Berlin, 2005.

[32]Mordukhovich, B. S., *Variational Analysis and Generalized Differentiation, II: Applications*, Springer, Berlin, 2005.

[33]Ross, I. M., " User's Manual for DIDO: A MATLAB Application Package for Solving Optimal Control Problems," Tech. Rep. 04-01.0, Naval Postgraduate School, Monterey, CA, December 2003.

List of Figures

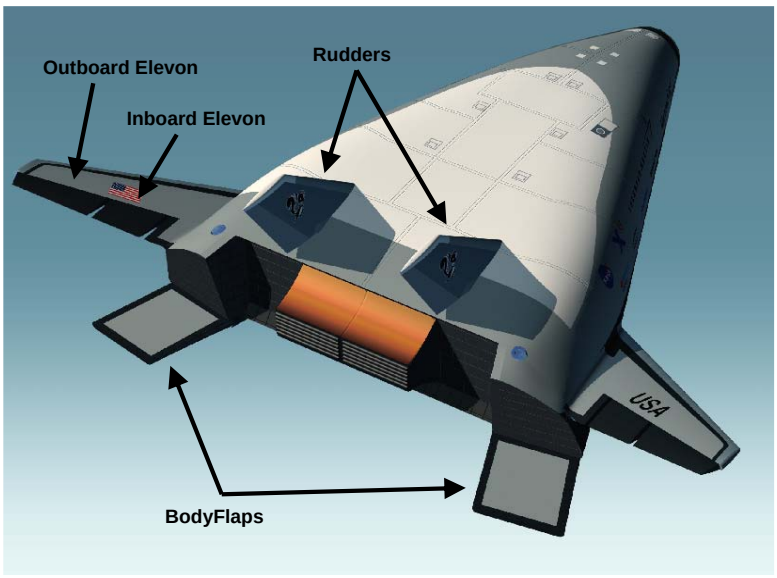

Figure 1: X-33.

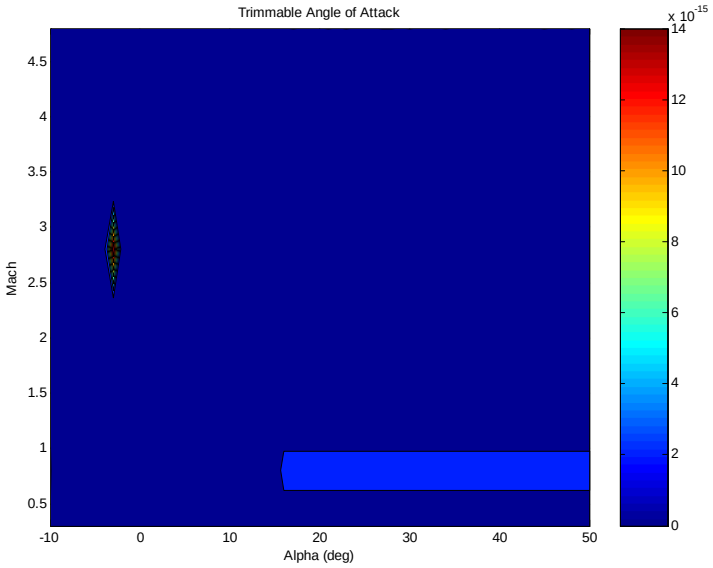

Figure 2: Pitch Deficiency For Nominal Vehicle.

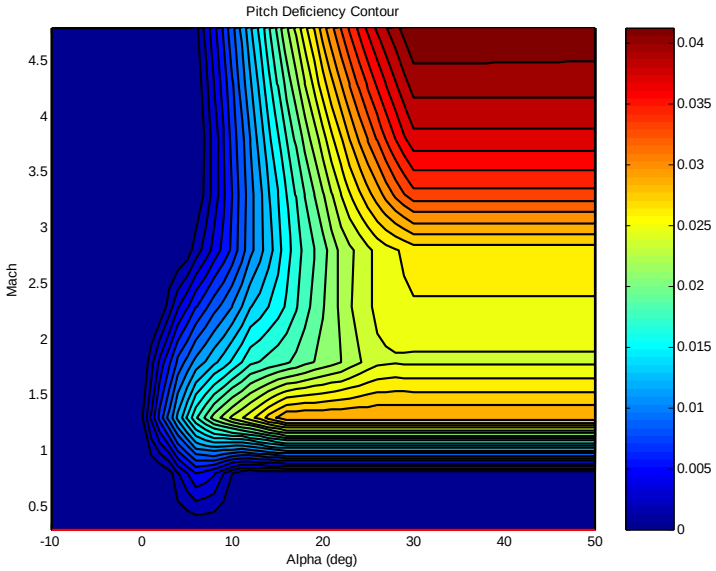

Figure 3: Pitch Deficiency For Failed Body Flaps at 26°.

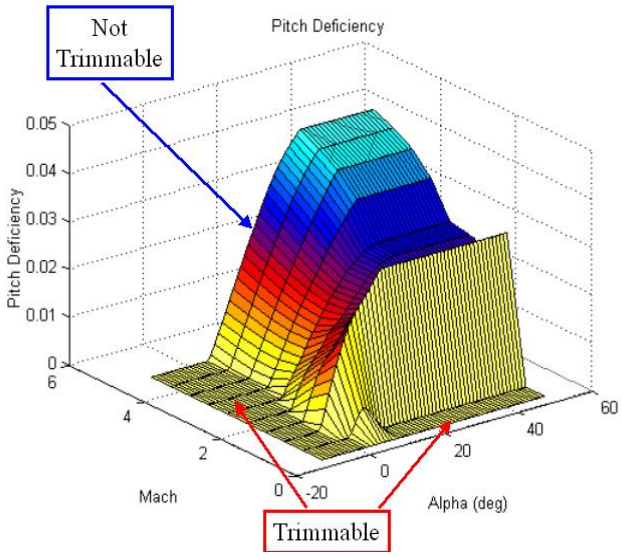

Figure 4: Three-Dimensional Pitch Deficiency For Failed Body Flaps at 26°.

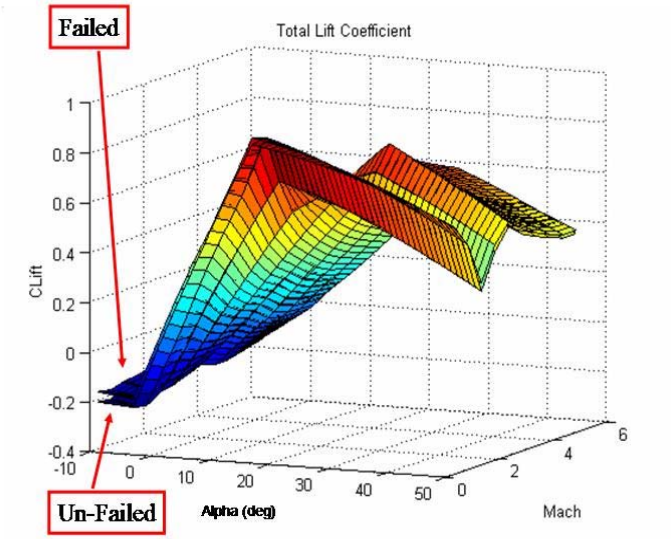

Figure 5: Nominal and Bodyflap Failure Lift Map.

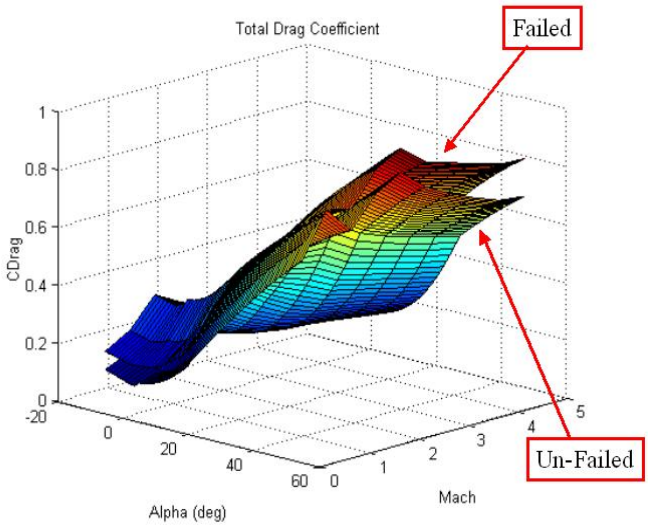

Figure 6: Nominal and Bodyflap Failure Drag Map.

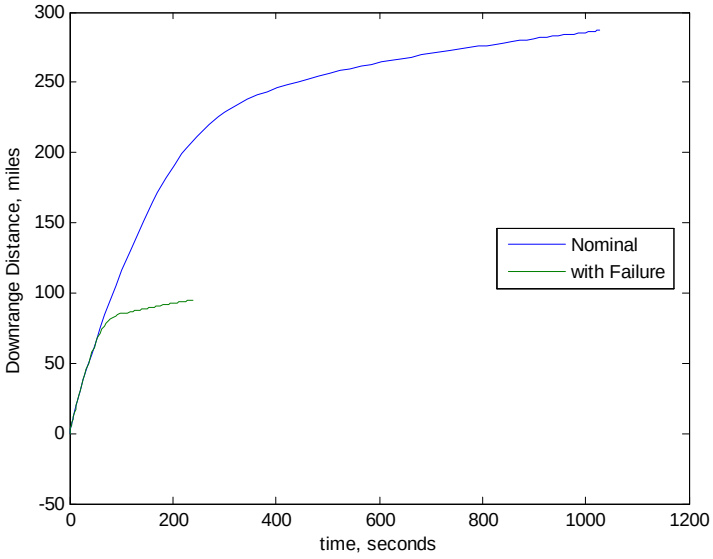

Figure 7: Downrange Profile.

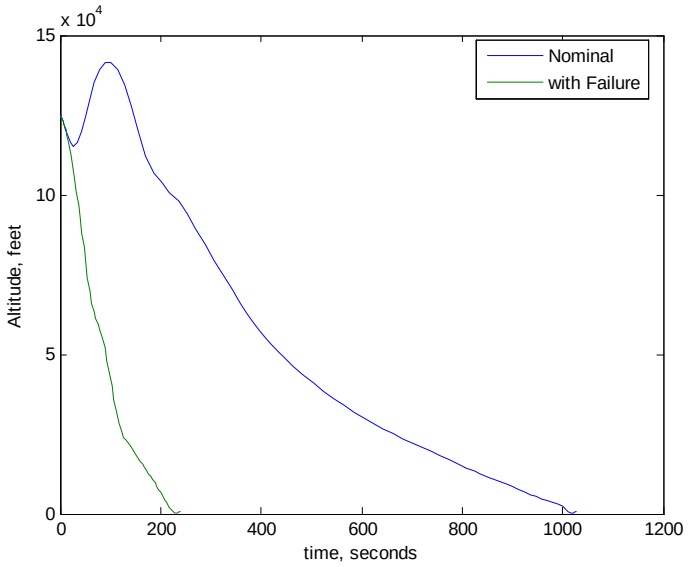

Figure 8: Altitude Profile.

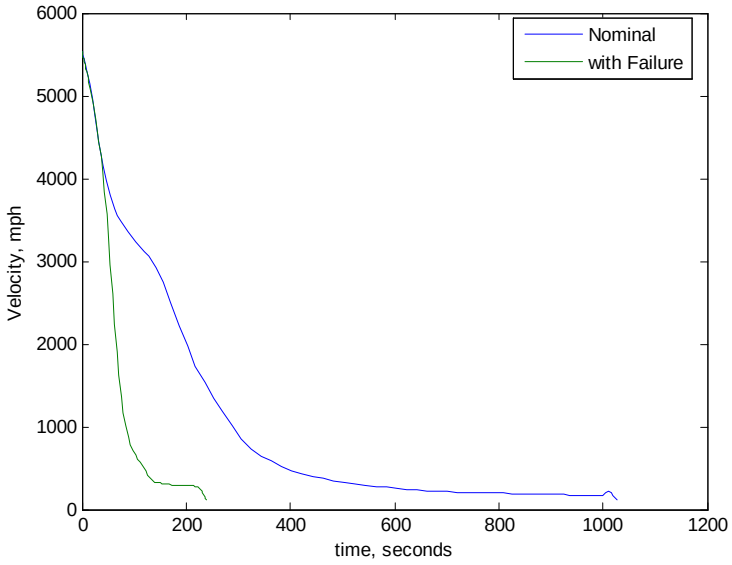

Figure 9: Velocity Profile.

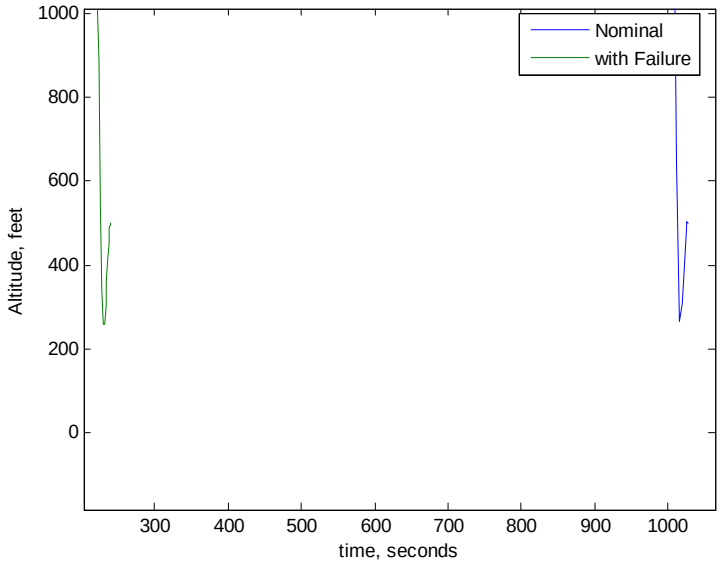

Figure 10: Altitude Profile.

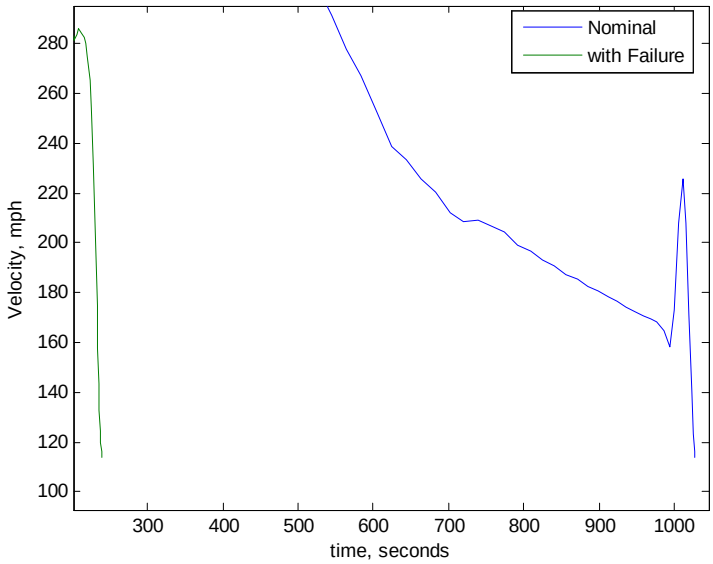

Figure 11: Velocity Profile.

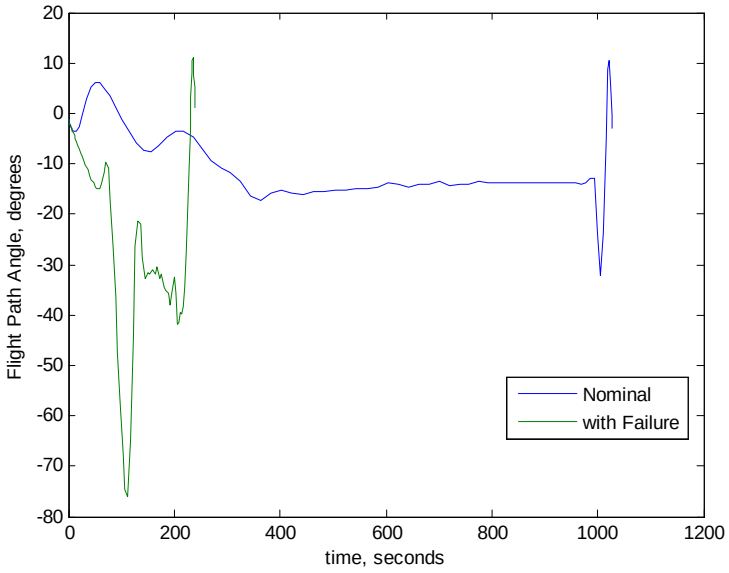

Figure 12: Flight Path Angle Profile.

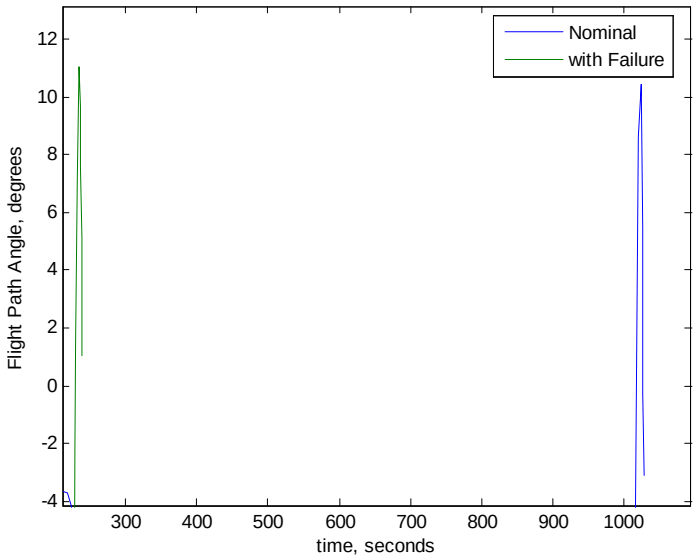

Figure 13: Flight Path Angle Profile.

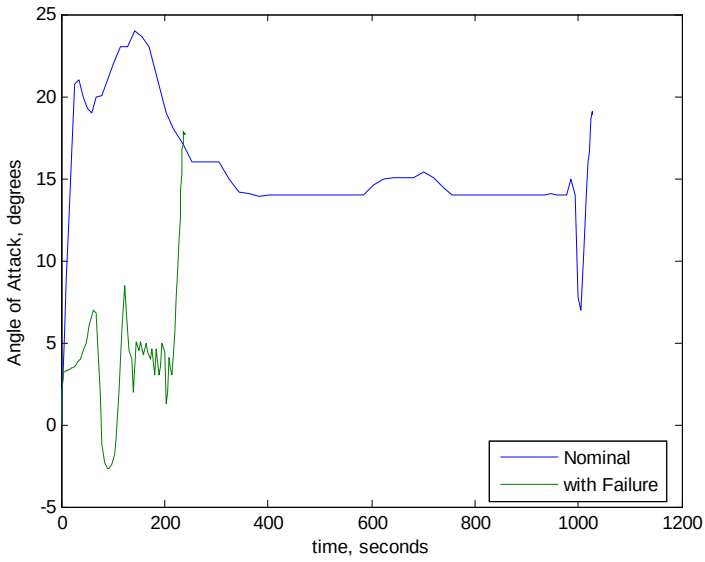

Figure 14: Angle of Attack Profile.

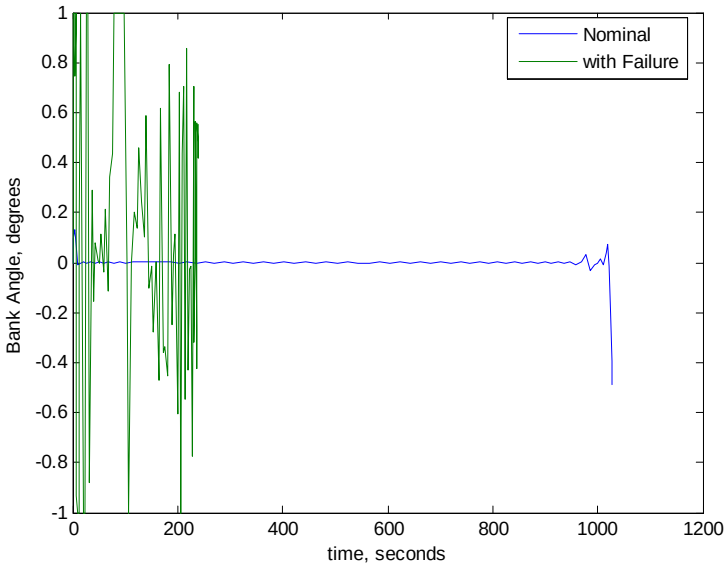

Figure 15: Bank Angle Profile.

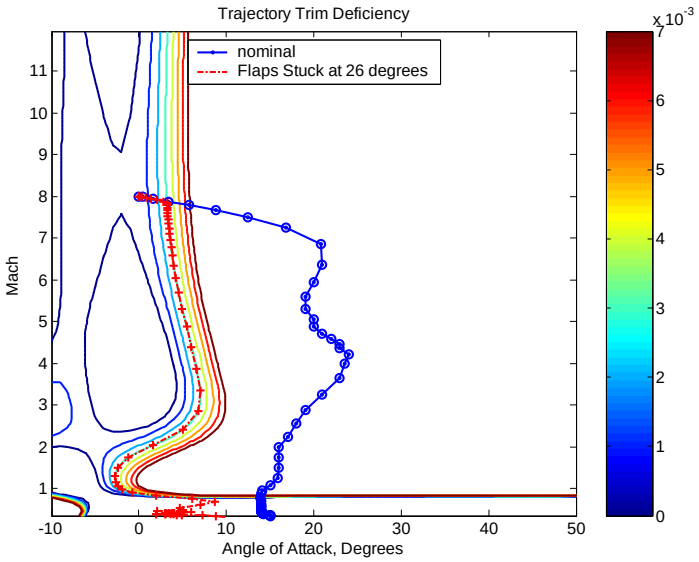

Figure 16: Trim Deficiency Map With Max Downrange Trajectories.